Published in final edited form as:
Nat Genet. 2016 November ; 48(11): 1349–1358. doi:10.1038/ng.3676.

Mutations in the HECT domain of *NEDD4L* lead to AKT/mTOR pathway deregulation and cause periventricular nodular heterotopia

Loïc Broix[#1,2,3,4,5], **Hélène Jagline**[#1,2,3,4], **Ekaterina Ivanova**[1,2,3,4], **Stéphane Schmucker**[1,2,3,4], **Nathalie Drouot**[1,2,3,4], **Jill Clayton-Smith**[6], **Alistair T. Pagnamenta**[7], **Kay.A. Metcalfe**[6], **Bertrand Isidor**[8], **Ulrike Walther Louvier**[9], **Annapurna Poduri**[10], **Jenny C. Taylor**[7], **Peggy Tilly**[1,2,3,4], **Karine Poirier**[5], **Yoann Saillour**[5], **Nicolas Lebrun**[5], **Tristan Stemmelen**[1,2,3,4], **Gabrielle Rudolf**[2,3,4], **Giuseppe Muraca**[5], **Benjamin Saintpierre**[5], **Adrienne Elmorjani**[5], **The Deciphering Developmental Disorders study**[11], **Martin Moïse**[12], **Nathalie Bednarek Weirauch**[13], **Renzo Guerrini**[14], **Anne Boland**[15], **Robert Olaso**[15], **Cecile Masson**[16], **Ratna Tripathy**[17], **David Keays**[17], **Cherif Beldjord**[18], **Laurent Nguyen**[12], **Juliette Godin**[1,2,3,4], **Usha Kini**[19], **Patrick Nischké**[16], **Jean-François Deleuze**[15], **Nadia Bahi-Buisson**[20], **Izabela Sumara**[1,2,3,4], **Maria-Victoria Hinckelmann**[1,2,3,4], and **Jamel Chelly**[1,2,3,4,21]

[1]Institut de Génétique et de Biologie Moléculaire et Cellulaire, Illkirch, France

[2]Centre National de la Recherche Scientifique, U7104, Illkirch, France

Corresponding author Jamel Chelly, MD, PhD, IGBMC, Department of Translational Medicine and Neurogenetics, 1, rue Laurent Fries, BP 10142, 67404 Illkirch Cedex, France, chelly@igbmc.fr.
A list of DDD study investigators and their affiliations appears in the Supplementary Note

URLs
The Exome Aggregation Consortium (*ExAC*): http://exac.broadinstitute.org/
Mutation Tester: http://www.mutationtaster.org/
DECIPHER: https://decipher.sanger.ac.uk/)
Epi4K Consortium: http://www.epgp.org/
Deciphering Developmental Disorders Study: http://www.ddduk.org/
SubRVIS: http://www.subrvis.org/

Accession Codes.
Human *NEDD4L* (NM_001144967), mouse *Nedd4l* (NM_0114386).
ClinVar accessions: SCV000267106 - SCV000267109
Exome sequencing data deposition: dbGaP (http://www.ncbi.nlm.nih.gov/gap) Study Accession: phs000653.v1.p1 for Pnh31124 trio (Proband id: EPGP012746). and EGAS00001000775 (www.ebi.ac.uk/ega/datasets/EGAD00001001848) for DDDP110533 trios.
For the other patients analyzed by WES approach, no consent was obtained from the patients to deposit the WES data in a repository.

Author Contributions
LB, HJ EI and MVH conceived and designed the experiments, performed the experiments, performed statistical analysis and analyzed the data related to cellular, *in utero* electroporation and functional studies. SS provided technical assistance and performed ubiquitination experiments. ND provided technical assistance and performed expression and genetic studies, and preparation of reagents. JCS, KAP, BI, UWL, AP, NBW, RG, DK, BC, DDD Study, UK and NBB contributed clinical and imaging data and follow up of patients and families. PT and GM provided assistance for in utero electroporation studies. ATP, JCT, JCT, KP, YS, NL, GR, BS, AE and RT contributed in genetic studies and analysis of variants in candidate genes and screened subjects DNA. MM, and JG performed expression studies during brain development. LN and JG contributed reagents and material, as well as critical suggestions for functional studies. TS, DDD study, AB, RO, CM, PN, JFD contributed in the generation of WES and bioinformatics tools and analysis of sequencing data. IS conceived and designed ubiquitination experiments. J.C. conceived, coordinated and supervised the study, designed experiments, analysed data and wrote the paper.

Competing Financial Interests
The authors declare no competing financial interests.

Europe PMC Funders Author Manuscripts

[3]Institut National de la Santé et de la Recherche Médicale, U964, Illkirch, France

[4]Université de Strasbourg, Illkirch, France

[5]Institut Cochin, Institut National de la Santé et de la Recherche Médicale U1016, Centre National de la Recherche Scientifique U 8104, Paris Descartes University, Paris, France

[6]Manchester Centre For Genomic medicine, Central Manchester University Hospitals National Health Service Trust, Manchester Academic Health Science Centre, Manchester, UK

[7]National Institute for Health Research Biomedical Research Centre, Wellcome Trust Centre for Human Genetics, University of Oxford, Oxford, UK

[8]Service de Génétique Médicale, University Hospital of Nantes, Nantes, France

[9]Unité de Neuropédiatrie et d'épileptologie infantile, University Hospital of Montpellier, Montpellier, France

[10]Epilepsy Genetics Program, Division of Epilepsy and Clinical Neurophysiology Department of Neurology, Boston Children's Hospital, Boston, MA, USA

[11] Deciphering Developmental Disorders Study, Wellcome Trust Sanger Institute, Hinxton, Cambridge, UK

[12]Grappe Interdisciplinaire de Génoprotéomique Appliquée- Neurosciences, University of Liège,, Liège, Belgium

[13]Hôpital Maison Blanche, University Hospital of de Reims, France

[14]Paediatric Neurology Unit, A. Meyer Children’s Hospital–University of Florence, Florence, Italy

[15]Centre National de Génotypage , Evry, France

[16]Institut Imagine, Bioinformatics Platform, Paris Descartes University, Paris, France

[17]Institute of Molecular Pathology, Vienna, Austria

[18]Laboratoire de biochimie et génétique moléculaire, Hôpital Cochin, Paris, France

[19]Department of Clinical Genetics, Oxford University Hospitals National Health Service Trust, UK

[20]Institut Imagine, Institut National de la Santé et de la Recherche Médicale U1163- Paris Descartes University, Hôpital Necker-Enfants Malades, Paris, France

[21]Service de Diagnostic Génétique, Hôpital Civil de Strasbourg, Hôpitaux Universitaires de Strasbourg, France

[#] These authors contributed equally to this work.

Abstract

Neurodevelopmental disorders with periventricular nodular heterotopia (PNH) are etiologically heterogeneous, and their genetic causes remain in many cases unknown. Here we show that missense mutations in the HECT domain of the E3 ubiquitin ligase NEDD4L lead to PNH associated with toes syndactyly, cleft palate and neurodevelopmental delay. Cellular and expression data showed a sensitivity of PNH-associated mutants to proteasome degradation. Moreover, *in utero* electroporation approach showed that PNH-related mutants and excess of wild

type (WT) NEDD4L affect neurogenesis, neuronal positioning and terminal translocation. Further investigations, including rapamycin based experiments, revealed differential deregulation of pathways involved. Excess of WT NEDD4L leads to a disruption of Dab1 and mTORC1 pathways, while PNH-related mutations are associated with a deregulation of mTORC1 and AKT activities. Altogether, these data provide insights to better understand the critical role of NEDD4L in the regulation of mTOR pathways and their contributions in cortical development.

Introduction

The development of the human cerebral cortex requires coordinated spatial and temporal regulation of interdependent developmental processes that include proliferation, migration and layering, as well as differentiation of distinct neuronal populations1,2. Disruption of any of these processes can result in a wide range of developmental disorders. Many of these disorders are classified within the group of malformations of cortical development (MCD) that includes lissencephaly, pachygyria, polymicrogyria (PMG), microcephaly and periventricular nodular heterotopia (PNH)3–5. MCD are often associated with severe intellectual disability (ID) and epilepsy, and their evolving classification is based on the developmental process thought to be first affected in combination with the underlying disrupted genes and biological pathways3.

Within the group of MCD associated with neuronal migration abnormalities, PNH represents about 31% of MCD (R.G. unpublished data). Anatomically, PNH is characterized by bilateral ectopic nodules of grey matter lining the lateral ventricles. Clinical presentations in patients with PNH are heterogeneous, though seizures and learning difficulties are the most common clinical features5.

So far, mutations in the X-linked filamin A (*FLNA*) gene6, encoding a widely expressed 280 kDa actin-binding phosphoprotein account for about 50% of bilateral PNH and the associated Ehler-Danlos conditions affecting mostly females7. Compelling studies suggested that FLNA-related PNH results from the combination of defects affecting the polarized radial glia scaffold and its adhesion to the neuroependymal membrane, neural progenitor proliferation and neuronal migration8–10. Other mechanisms contributing to PNH pathogeny were proposed following the identification of rare familial forms of PNH associated with recessive mutations in *ARFGEF2* encoding the ADP-ribosylation factor guanine exchange factor 211. Finally, other genetic forms of PNH have been mapped through comparative genomic hybridization array studies, but only one potential causal gene, *C6orf70* (*ERMARD*) located in 6q27 region, has been identified12.

Here we provide evidence implicating E3 ubiquitin ligase NEDD4L in the pathogeny of PNH. We report the identification of missense mutations in the *NEDD4L* gene in patients with PNH, bilateral syndactyly, cleft palate and neurodevelopmental delay. We further show that PNH-related NEDD4L mutants disrupt neurodevelopmental processes likely through dysregulation of mTOR and AKT signalling pathways.

Europe PMC Funders Author Manuscripts

Results

Patients with PNH analyzed by WES and mutations in *NEDD4L*

We used clinical and brain MRI data of patients with MCD referred for genetic investigations and selected 15 patient-parent trios for analysis by whole exome sequencing (WES). All families had a single affected patient with bilateral PNH. For WES approach, we applied previously described experimental workflow to detect, prioritize sequence variants and validate significant findings13,14. We then analyzed filtered exome data and searched for recurrence of *de novo* mutations in the same gene in unrelated patients. We identified *de novo* missense changes in *NEDD4L* in two patients with bilateral contiguous PNH, bilateral syndactyly of the 2/3 toes and neurodevelopmental delay (P158 and BRC217; Table 1, Fig. 1a,b and Supplementary note). Following validation of the mutations by Sanger sequencing (Supplementary Fig. 1a,b), we screened *NEDD4L* (coding exons and their flanking sequences) in a cohort of 96 patients with MCD and identified the c.2677G>A mutation (already detected in BRC217) in one additional patient (P347; Table 1, Fig. 1c and Supplementary Fig. 1c). Interestingly, the phenotype of this patient is also characterized by a bilateral PNH, bilateral syndactyly of the 2/3 toes and neurodevelopmental delay (Table 1 and Supplementary note). As the family of patient P347 consists of two affected children (P347 and her brother), a healthy girl and healthy parents (Supplementary Fig. 1c), we tested the segregation of the variant in all members of the family. We found the variant to be present in a heterozygous state in the affected brother, but absent from the DNA of the healthy sister and father. For the mother, however, sequencing traces consistently revealed a significant imbalance in peak heights corresponding to normal and variant alleles (Supplementary Fig. 1c). Altogether, these results were suggestive of germline and somatic mosaicism of *NEDD4L* variant in the mother. In order to confirm and evaluate the level of somatic mosaicism, we analyzed the mother's DNA by digital droplet PCR and found that the mutated allele frequency is around 16% (Supplementary Table 1). In view of these molecular data the mother was re-examined and neurological, cognitive and behavioural evaluations were found normal.

Shortly after these initial findings, we reinforced the implication of *NEDD4L* by the identification of additional *de novo* mutations in three unrelated patients with PNH (Table 1). The first patient (PNC: Fig. 1d, Table 1 and Supplementary Fig.1d) was identified through targeted screening of a MCD-related panel of genes in which we included *NEDD4L*. The second and third patients: DDDP110533 (Fig. 1e, Table 1 and Supplementary Fig. 1e) and Pnh31124 (Table 1 and Supplementary Fig. 1f), were identified through data sharing of trios exome sequenced and analyzed as part of the Deciphering Developmental Disorders and the Epi4K Consortium studies. For all three patients, brain MRI also revealed the presence of PNH associated with syndactyly and neurodevelopmental delay (Fig. 1d,e, Table 1 and Supplementary note).

NEDD4L gene15 (also known as *NEDD4-2*) encodes for a member of the NEDD4 family of HECT-type E3 ubiquitin ligases known to regulate the turnover and the function of a number of proteins involved in fundamental cellular pathways and processes16–19. Interestingly, all mutations associated with PNH are located in the HECT domain (Fig. 1f) and relevance of

their pathogenic effect was suggested by the high degree of conservation of the affected residues (Supplementary Fig. 2a), bioinformatics predictions (i.e., Mutation Tester tool), and structural modelling of the HECT domain (Supplementary Fig. 2b-j).

Functional effects of WT *NEDD4L* and *NEDD4L* mutations

We first analyzed the expression of *Nedd4l* during mouse brain development. As illustrated in Supplementary Figure 3a (*in situ* hybridization at E15), *Nedd4l* transcripts are homogenously distributed in the cortical plate, ventricular zone and ganglionic eminences. Moreover, analysis of *Nedd4l* expression by real time quantitative PCR in developing mouse cortex from E12.5 to E18.5 showed a peak of expression at E16.5 (Supplementary Fig. 3b), a developmental stage characterized by both proliferation and migration.

To assess cellular consequences of PNH-related mutations, we transfected WT and three different mutant versions of *NEDD4L* cDNA constructs, and compared their expression level and localization by immunofluorescence (Fig. 2). We found that WT NEDD4L was highly expressed (Fig. 2a and Supplementary Fig. 4), and its localization is in line with what was previously reported20. In contrast, PNH-related mutant proteins were hardly detectable. Indeed, 48h after transfection we only detected a faint signal comparable to the background signal of cells transfected with the control empty vector (Fig.2a). Similar results were observed upon transfection of primary cultured neurons (Supplementary Fig.4). We also confirmed the lack of NEDD4L mutants expression by Western blot using protein extracts from transfected N2A cells (Fig. 2b). In view of these results, we hypothesized that PNH-associated mutants are unstable and examined NEDD4L protein expression in transfected cells treated with the proteasome inhibitor, MG132. As illustrated in figure 2 (Fig. 2a,b), we observed by immunofluorescence and Western blot experiments a significant level of expression of PNH-related NEDD4L mutants.

To further ascertain that NEDD4L mutants instability represent a disease relevant phenotype we tested the expression of three control variants reported in ClinVar and/or Exac databases. Referring to NM_001144967, these variants are: c.698C>T, pSer233Leu; c.535T>A, p.Ser179Thr and c.2614G>A, p.Gly872Ser (located in the HECT domain). As illustrated in Supplementary figure 5a,b, cellular localization and expression level of the different control version of NEDD4L cDNA constructs are similar to those of WT NEDD4L.

To strengthen the implication of a post-transcriptional mechanism, we analyzed the expression of *NEDD4L* transcripts by quantitative RT-PCR using the co-transfected reporter GFP as normalizer. We found that WT *NEDD4L* transcript level was approximately 1.5 to 2 fold higher than mutant levels (Supplementary Fig. 6), a range of difference that does not explain the almost complete absence of mutant proteins.

Since all mutations are located in the catalytic HECT domain of the NEDD4L E3-ligase and lead to protein instability, we sought to assess consequences of disease-causing variants on enzymatic activity and self-ubiquitination. To this end we focused on Arg897Gln mutation and compared by two different approaches the ubiquitination ability of WT and NEDD4L mutant.

First, to test specifically for NEDD4L ubiquitination, we transfected N2A cells with N-terminal V5-tagged *NEDD4L* cDNA constructs, immunoprecipitated NEDD4L from lysates using anti-V5 antibodies and immunoblotted with an anti-ubiquitin antibody to detect conjugation of ubiquitin. Long exposure times of Western blots showed a high-molecular mass smear mainly representing self-ubiquitinated WT and NEDD4L mutant. Interestingly, despite the instability of the V5-tagged mutant protein and its low amount, the intensity of the smear detected by anti-ubiquitin antibodies is comparable to that of the WT (Supplementary Fig. 7a).

Second, we compared ubiquitination ability of immunopurified V5-tagged NEDD4L (WT and mutant) in an *in vitro* assay using recombinant E1 and E2 (UbcH7) enzymes with or without ubiquitin. As shown in Supplementary Figure 7b, in the presence of ubiquitin both WT and mutant NEDD4L exhibit ubiquitination activity illustrated by the high-molecular mass smear detected by anti-NEDD4L antibodies.

To further confirm and better visualize ubiquitination activity of NEDD4L mutant we performed another series of immunoprecipitation and *in vitro* assays and WB analyses in which we loaded four times less of protein products corresponding to the assay with WT NEDD4L than to the one with NEDD4L mutant (Fig. 3). Though accurate comparison of WT and mutant NEDD4L ubiquitination activities is difficult, both immunoprecipitation (Fig. 3a) and in vitro ubiquitination (Fig. 3b) approaches showed that NEDD4L mutant induced a high-molecular mass smear detected with anti-V5 and anti-NEDD4L antibodies.

Altogether these results suggest that ubiquitination activity of NEDD4L mutant is preserved and possibly enhanced if we take into account the significant level of ubiquitination activity despite the instability of the protein.

At first sight, the fact that PNH-related NEDD4L mutants are unstable led us to consider haplo-insufficiency mechanism. However, previously reported findings and our data made this hypothesis questionable. For instance, post-mitotic neurons deficient for both *Nedd4-1* and *Nedd4l* (analyzed in conditional double KO mice), migrate properly to the cortical plate21. Also, neuronal migration disorders and PNH are not among the features associated with haploinsufficiency resulting from heterozygous CNVs reported in DECIPHER databases . Moreover, 3 frameshift and 1 stop gained mutations were reported in the data set of Exome Aggregation Consortium in which individuals affected by severe paediatric disease have been excluded. Finally, we used *in utero* RNA interference approach to analyze the consequences of *Nedd4l* downregulation on cortical neuronal migration in mice, and found no significant difference between embryo brains transfected with shRNA targeting *Nedd4l* and scrambled shRNA control (Supplementary Fig.8a,b).

In view of these convergent arguments, we then sought to study the consequences of PNH-related mutations on neurodevelopmental proceses. We used *in utero* electroporation (IUEP) approach and compared the consequences of WT and NEDD4L mutants (p.Glu893Lys and p.Arg897Gln) expression on neuronal positioning, neuronal progenitor proliferation and terminal translocation. To assess effects on projection neurons positioning we electroporated *NEDD4L* constructs in combination with Tomato reporter construct into progenitor cells

located in the VZ of E14.5 mouse neocorticies and analyzed brain embryos four days later (E18.5). In E18.5 brain sections, we observed that neurons electroporated with the empty vector reached the cortical plate (CP) (Fig. 4a,b). However, IUEP of WT *NEDD4L*, and PNH-related mutants induced a significant arrest of cells within the ventricular/sub-ventricular zone (VZ/SVZ) and intermediate zone (IZ) with a corresponding depletion in the CP (Fig. 4a,b). We also assessed the effect on neuron positioning at postnatal day 2 (P2) and highlighted differences that parallel those observed at E18. While neurons electroporated with empty vector were mainly located in the superficial layers II-IV of cortical plate, we found that neurons electroporated with WT and PNH-related *NEDD4L* mutants were abnormally distributed in the white matter and in layers V and VI of the CP(Supplementary Fig. 9a,b).

As our cellular data suggested that PNH-related NEDD4L mutants are unstable, we also assessed whether the same effect could be observed *in vivo* in electroporated migrating neuronal cells. As illustrated in Figure 4c and Supplementary Figure 9c, we found that cells electroporated with WT *NEDD4L* exhibit a strong cytoplasmic immunolabelling, consistent with a high level of NEDD4L expression. However, in neurons electroporated with mutated constructs, we only detected a faint signal that could correspond to the endogenously expressed NEDD4L (Fig. 4c and Supplementary Fig. 9c).

To study terminal translocation22–25 we conducted IUEP of the different constructs at E14 and collected 6 days later (P2) brains from the pups. We then assessed the distribution of electroporated neurons with a leading process adhering to the ECM in the region previously defined as the primitive cortical zone (PCZ)24, and in up and down Cux1 regions corresponding to two equal parts of the remaining Cux1-positive layer (Supplementary Fig. 10). We found that expression of WT and NEDD4L mutants led to an abnormal distribution of neuronal cells with a deviating enrichment in down Cux1 region (Supplementary Fig. 10), suggesting that terminal translocation was disrupted.

To test consequences of *NEDD4L* mutations on apical and basal progenitor proliferation, we performed IUEP at E14 and collected embryos 48 h later for immunohistochemistry using antibodies against PH3, Pax6, Tbr2 and Ki67. We found a significantly higher percentage of tomato-positive and PH3-positive co-labelled cells expressing WT or HECT mutants in the VZ when compared to tomato-positive cells expressing the control empty vector (Fig. 4d and Supplementary Fig. 9d). These results suggested an increased mitotic index of apical progenitors electroporated with WT and PNH-related mutations. We also quantified electroporated Pax6-positive and Tbr2-positive cells in VZ and SVZ and found an increased number of these cell populations only in brain embryos electroporated with PNH-related mutant constructs (Fig. 4e and Supplementary Fig. 9e).

To assess the pool of proliferating cells, we evaluated double Tomato and Ki67 positives cells in VZ and SVZ and in both regions we didn’t observe any differences following electroporation of control empty vector, WT *NEDD4L*, and mutant *NEDD4L* cDNA constructs. (Supplementary Fig. 9f,g).

We also performed immunohistochemistry against Cux1 marker at E18.5 and observed that arrested neurons electroporated with WT *NEDD4L*, or PNH-related mutants express Cux1 indicating that misplaced neurons in deep layers of the cortex are differentiated and fated for the upper layers (Supplementary Fig. 9h).

Finally, we labeled brain slices (E16.5 and E18.5) with the anti-cleaved caspase-3 antibody to evaluate cell death rate and found no difference following electroporation with the different constructs (data not shown).

Pathways disrupted by WT NEDD4L and mutants causing PNH

Though the best known target of NEDD4L is the epithelial sodium channel (ENaC) shown to be involved in Liddle syndrome, a hereditary hypertension caused by elevated ENaC activity26, compelling evidences demonstrating crucial regulatory roles of NEDD4L in developmental processes have recently emerged19,27. In this study we sought to investigate consequences of WT and NEDD4L mutants on mTOR-dependent pathways for the following main reasons. First, in view of the association of MCD and distal limb abnormalities observed in patients described in this study, we wondered if these developmental abnormalities would not be a particular condition of the wide range of developmental brain and body disorders caused by dysfunctions of the interdependent phosphatidylinositol-3 kinase (PI3K)-AKT-mTOR pathways5,14. Second, among the many identified signalling pathways that modulate neuronal migration, the recently reported insights linking neuronal migration deficit of tuberous sclerosis complex (TSC) pathology with a cascade involving mTOR signalling, E3 ubiquitin ligase Cul5 expression and Dab1 expression28 also led us to consider a potential effect of NEDD4L on mTOR and Dab1 signalling pathways. Third, NEDD4L was recently identified as a critical player in the regulation of the crosstalk between PI3K/mTORC2 and TGFβ/activin/Smad2/3 signalling pathways29,30.

Therefore, we first tested by cellular and Western blot assays the effect of WT and NEDD4L mutants on mTORC1, AKT and Smad2/3 signalling activities. As illustrated in figure 5, following transfection in N2A cells of WT *NEDD4L* and PNH-associated mutants, we observed an increased level of phosphorylated S6 (pS6 at Ser240/244) that reflects elevated mTORC1 signalling activity (Fig. 5a,c). In contrast, for AKT, only PNH-associated NEDD4L mutants are associated with significantly increased level of Thr308 and Ser473 phosphorylated forms of Akt (Fig. 5b,c).

To reinforce relevance and specificity between NEDD4L mutants expression and the above highlighted findings, we tested the effect of the three control variants on S6 and AKT phosphorylation and found that overexpression of the three NEDD4L variants is associated with a phosphorylation pattern that is similar to the one of WT NEDD4L (Supplementary Fig. 5b).

For Smad 2/3 activities, we tested the effect of WT and Arg897Gln NEDD4L mutant in basal condition and upon activation of TGF-β pathway by activin A (AA) on the expression levels of Smad2-pSer465/467, Smad3-pSer423/425 and Akt-pSer473. In basal condition we found that overexpression of WT NEDD4L had no effect on the activation level of Smad2/3

factors, while expression of mutant NEDD4L is associated with a significant increase of phospho-Smad2/3 levels (Supplementary Fig. 11). Upon activation by AA of TGF-β pathway we found that overexpression of WT NEDD4L is associated with an increase of phospho-Akt and phospho-Smad2/3 levels, while expression of NEDD4L mutant is associated with a significant decrease of phospho-Akt level and stable levels of phospho-Smad2/3 (Supplementary Fig. 11). Collectively, these results suggested that expression of NEDD4L mutant lead to a disruption of the regulated cross talk between Akt and Smad2/3 signalling in activin/TGF-β pathways.

In order to assess the *in vivo* contributions of these pathways in the developmental defects described above, we used IUEP approach in combination with rapamycin treatment (a well-known mTORC1 inhibitor) of the pregnant mice and analyzed the effect on projection neurons positioning. Interestingly, in E18 brain sections of embryos electroporated at E14 with WT *NEDD4L* and subjected to rapamycin treatment we found a clear rescue of neuronal positioning defect with a distribution of electroporated cells across the cortex similar to the control empty vector (Fig. 6a,b). For this latter condition, the distribution of neuronal cells with or without rapamycin treatment was similar (Fig. 6a,b). However, rapamycin treatment induced only a partial rescue of the neuronal position defect resulting from IUEP of PNH-related mutants (Fig. 6a,b). We found that the number of Tomato-positive neurons with delayed migration was reduced in the IZ, while the number of neurons that reached the CP was significantly increased (Fig. 6a,b). We also analyzed the expression of NEDD4L in neuronal cells that reached the cortical plate after rapamycin treatment and found an absence of NEDD4L expression in neurons electroporated with PNH-associated mutants (data not shown), while neurons electroporated with WT NEDD4L still expressed a high level of NEDD4L (Supplementary Fig. 12).

We then analyzed brain sections by immunohistochemistry using antibodies against Dab1 and assessed whether rapamycin-rescued neuronal position correlates with relevant changes of Dab1 expression and distribution in electroporated neurons. In arrested neuronal cells electroporated with WT *NEDD4L*, we found a striking labelling suggesting an enrichment and an almost exclusive localization of Dab1 in the periphery of the cytoplasm, a distribution pattern that is easily distinguishable from the diffuse pattern found in neurons electroporated with empty vector or mutant constructs (Fig. 6c). Interestingly, following rapamycin treatment, in the predominant pool of neurons that reached the CP and that still express a high level of WT NEDD4L, we found a restoration of the diffuse pattern of Dab1 localization (Fig. 6c). However, in neurons electroporated with PNH-associated mutants, no significant change in Dab1 cellular localization was observed neither in the misplaced, nor in the rescued neurons that reached the cortical plate (Fig. 6c).

Discussion

Findings presented herein demonstrate the critical role of NEDD4L in the regulation of processes involved in cortex development, and implicate mutations in the HECT domain of NEDD4L in PNH. Indeed, we report the identification of 5 *de novo* and one transmitted mutation in 7 patients (two sibs and 5 unrelated patients) with a common distinguishable phenotype characterized by PNH, ID cleft palate and syntactyly (in 6 out of 7 patients). All

mutations associated with this phenotype are located in the HECT domain of the E3 ubiquitin ligase of NEDD4L, and one of these muations, c.2677G>A, p.Glu893Lys, is a reccurrent mutation that was found in three unrelated families (Table 1).

One of the intriguing effects of PNH-related mutations was the likely increased sensitivity of the mutants to proteasome degradation. To explain this sensitivity, we propose the hypothesis illustrated by the model depicted in figure 7a. Mutations causing amino acids changes in the HECT domain could lead to conformation changes and constitutive activation of the catalytic function, which in turn could trigger auto-ubiquitination of NEDD4L mutants and their degradation. This hypothesis is based on previously reported studies suggesting that catalytic activity, including auto-ubiquitination of HECT E3 ligases, is dependent on NEDD4L conformations31–34.

With the model of constitutive activation due to mutations in the HECT domain, one could expect not only auto-ubiquitination, but also aberrant ubiquitination of other NEDD4L substrates, while conventional loss-of-function mechanism is expected to lead to a deficit of the ubiquitination activity. Moreover, despite its auto-ubiquitination and degradation, the predicted state of constitutive activation of NEDD4L mutants could mimic the increased activity resulting from the overexpression of WT NEDD4L. This model could therefore reconcile, at least partially, the apparent discrepacy regarding the observed similar neurodevelopmental defects resulting from the IUEP of the stable WT NEDD4L and the unstable NEDD4L mutants.

Another finding that was observed with WT and NEDD4L mutants corresponds to positioning defect of post-mitotic neuronal cells. Interestingly, in the misplaced neuronal cells overexpressing WT NEDD4L, we observed a striking pattern of Dab1 distribution. It is worth mentioning that this finding is in line with previously reported studies that demonstrated the association between the excess of the nucleocytoplasmic Dab1 in the cytoplasm of postmitotic neurons and its inhibitory effect on neuronal migration35. In arrested neuronal cells electroporated with NEDD4L mutants the unchanged distribution of Dab1 suggest that neuronal migration defect caused by NEDD4L mutants could be underlined by a mechanism that is divergent from the one disrupted by the overexpression of WT NEDD4L. In favour of this are the evidences suggesting that excess of WT NEDD4L is associated with a disruption of signalling pathways regulated by mTORC1 and Dab1, while PNH-related mutants might act through deregulation of mTORC1, Akt, mTORC2 and TGF-β/Smad2/3 pathway activities (Fig. 7b). Though further investigations are required to define the exact mechanisms by which NEDD4L overexpression and mutants affect these pathways, these hypotheses are supported by a recent study showing that NEDD4L catalyzes ubiquitination of PIK3CA and regulates PI3K-AKT signaling35, and our rapamycin-based experiments. Indeed, the consistent rescue of neuronal position defect and restoration of cellular distribution of Dab1 by rapamycin treatment suggest that migration and positioning defects induced by the overexpression of WT NEDD4L could be mediated by mTORC1 pathways deregulation.

For PNH-related mutants, in addition to the increased activity of mTORC1, the deregulation of Akt and Smad2/3 activities in basal conditions and upon TGF-β activation provide an

interesting entry point to further understand the role of NEDD4L in the regulation of neurodevelopmental processes underlying cortical development and the established implication of PI3K/AKT signalling pathways in a large spectrum of neurodevelopmental syndromes caused by activating mutations in AKT3, PIK3R2 and PIK3C, some of which are associated with phenotypic features of MCD5,14,36,37.

As a whole and to the best of our knowledge, we have for the first time showed that mutations altering the HECT domain of NEDD4L are associated with PNH and excess of NEDD4L is likely to be deleterious for brain development and functioning. This latter finding provides therefore a basis for a better understanding of phenotypes associated with duplications encompassing NEDD4L. In this study we also reported evidence highlighting disruptive consequences of NEDD4L mutations on AKT/mTOR and TGF-β/Smad2/3 signalling pathways. Moreover, our study revealed a potential novel disease-causing molecular mechanism, where missense mutations might lead to a constitutive active state and loss of the mutant protein, but with functional consequences that are different from constitutive haploinsufficiency.

Online Methods

Subjects, WES and variants validation

Blood or DNA samples from affected individuals and their parents, and informed consent were obtained from all participants in accordance with the site-specific Institutional Review Boards. Written consent was obtained to publish patient photographs. For the selected 15 patients with periventricular nodular heterotopia (PNH) in association with either developmental delay and/or epilepsy, 3 out of the 15 patients have also polymicrogyria (PMG). For all patients, mutations in known PNH genes (*FLNA*, *ARFGEF2* and *C6orf70*) and pathogenic copy-number variations (CNVs) had been previously excluded. DNA processing, library generation, exome enrichment and WES in trios made of affected subjects and their parents were performed and analyzed at the French National Centre for Genotyping (CNG, Evry, France), Paris Descartes Bioinformatics platform and Sanger Sequencing Centre as previously described13,14,38. Available genomic databases (dbSNP, 1000 genomes, Exome Variant Server, the Exome Aggregation Consortium and a local Paris Descartes Bioinformatics platform database) were used to filter exome variants and exclude variants with a frequency greater than 1%. *De novo* variants were analyzed by PCR and direct Sanger sequencing using DNA from patients and their parents. In the family with two affected sibs and suspected maternal somatic mosaicism, confirmation and estimation of the percentage of cells bearing the variant was performed by Droplet Digital PCR approach (QX100 Droplet Digital PCR System, Bio-Rad Life Science Research, Hercules, CA, USA) using DNA extracted from peripheral blood of the all members of the family (the two patients, the parents and the non affected individual) and primers specific to variant and WT sequences. Data were analyzed with QuantaSoft v.1.4 software (Bio-Rad Life Science Research).

Protein modelling

Amino acid substitutions were plotted on the solved protein structure for the human Catalytic Domain of the Human NEDD4-like E3 Ligase using Phyre web portal (http://www.sbg.bio.ic.ac.uk/phyre2/). Models were built by homology modelling using Research Collaboratory for Structural Bioinformatics PDB code 2ONI. Images in Supplementary Figure 2 were rendered using Chimera.

Cloning and Plasmid constructs

Human untagged *NEDD4L* cDNA (NM_001144967.1) cloned in pCMV6-Entry vector (SC326303) was purchased from Origene. Mutations were introduced by site directed mutagenesis using QuikChange Site-Directed Mutagenesis Kit (Agilent Technologies). WT and mutated cDNAs encoding human NEDD4L were then inserted in the multiple cloning site of psiSTRIKE vector under the CAG promoter, pCDNA3-nV5. For *in utero* electroporation experiments, psiSTRIKE-*NEDD4L* vectors were electroporated in combination with a pCAGGS-IRES-Tomato vector to visualize electroporated cells.

For RNAi experiments, a 29-mer sequence targeting mouse *Nedd4l* mRNA and a HuSH 29-mer non-effective shRNA scrambled cassette, both commercially designed and provided by Origene in the p-GFP-V-RS vector (TG505433), were then inserted in psiSTRIKE vector under the U6 promoter. The *Nedd4l* shRNA directed against coding sequence was checked for specificity in sequence databases. Because of the very low level of expression of NEDD4L, efficiency experiments were conducted using co-transfection of WT NEDD4L cDNA and shRNA constructs in N2A cells and Western blot analysis.

In situ hybridization

Mouse *Nedd4l* sense and antisense probes (nt 462 to 1470 of the transcript NM_0114386) were synthesized using a T7 RNA polymerase (Roche) from pJET2.1-*Nedd4l* (nt 462 to 1470) and pJET2.1-*Nedd4l* (nt 1470 to 462) plasmids. Non-radioactive RNA *in situ* hybridization on frozen brain sections was performed as previously described39.

Quantitative reverse transcriptase-PCR (qRT-PCR)

Total RNA was prepared from brains of mouse embryos at different time points of development, and from cultured transfected cells with TRIzol reagent (Thermo Fisher Scientific) and cDNA samples were synthetized with SuperScript II Reverse Transcriptase (Invitrogen). Quantitative RT-PCR was performed in a lightCycler PCR Instrument (Roche) using SYBR Green Master Mix (Roche). For transfection-based experiments, we used GFP as normalizer (that is systematically co-transfected as reporter). For qRT-PCR of transcripts expressed by transfected cDNA constructs, RNA samples were treated with Turbo DNases (Ambion, Life Technology) to avoid amplification from plasmid DNA. Also, to ensure that we amplify transcripts expressed from transfected constructs, for each sample, real-time q-PCR (triplicates) was performed using cDNA reaction products obtained with or without reverse transcriptase, *NEDD4L,* and GFP specific primers.

Cell culture, transfections and immunofluorescence

N2A cells were cultured in Dulbecco's modified Eagle's media (Gibco) supplemented with 5% FCS and transfected using lipofectamine 2000 (Invitrogen). MG132 (Calbiochem BIO-TECHNE- R&D SYSTEMS EUROPE) was dissolved in DMSO solution buffer. DMSO was used as a control vehicle. Cells were treated with MG132 at 10 μM during 15 hours before the end of the culture. Expression of transfected genes was analyzed 48h post transfection by immunocytochemistry and western blot.

For primary cultures of neuronal cells, embryonic mouse cortical neurons (E17) were electroporated using Amaxa mouse Nucleofector kit (Lonza) and maintained in Neurobasal medium supplemented with 2% B27, 1% glutamine, 1% penicillin/streptomycin. Cells were fixed in 4% w/v paraformaldehyde (PFA) 96h after electroporation. Immunocytochemistry was performed according to standard procedures using anti-Nedd4l (13690-1-AP, rabbit, Proteintech, 1:200) was used as primary antibody and donkey anti rabbit IgG 647 (A-21208, Life Technologies, 1/800) as secondary. Results were observed and photographed using TCS SP5 confocal microscope, (Leica Microsystems).

Immunoblotting

Cells were lysed in RIPA buffer (50mM Tris HCl, pH 7.7; 0.15M NaCl; 1mM EDTA; 1% Triton X-100) supplemented with protease inhibitors (Roche) and phosphatases inhibitors (Sigma Aldrich). Protein concentration was measured using Bio-Rad protein assay reagent (Biorad Laboratories, CA). Samples were denatured at 95°C for 10 min in loading buffer then resolved in SDS-PAGE and transferred onto nitrocellulose membranes. Membranes were then blocked in 5% non-fat milk in TBS buffer, 0.1% Tween and then immunoblotted using the following primary antibodies in the specified concentrations: anti-Nedd4l (13690-1-AP, rabbit, Proteintech, 1:1000), anti-Actin (mouse, IGBMC, 1:1000), anti-Akt-pS473 (#4060, rabbit, Cell Signalling, 1:1000), rabbit anti-Akt-pT308 (#2965, rabbit, Cell Signalling, 1:1000) anti-Akt (pan) (#4691, rabbit, Cell Signalling, 1:1000), p-S6S236/236 (#2211, rabbit, Cell Signalling, 1/1000), anti-S6 (#2217, rabbit, Cell Signalling, 1:1000), anti-Ub (sc-8017, mouse, Santa Cruz, 1:250), anti-V5 (R96025, mouse, Invitrogen, 1:5000). All WB experiments consist of at least 3 independent replicates.

Immunohistochemistry

Mouse embryo brains were fixed by incubation overnight at 4°C in 4% w/v paraformaldehyde (PFA) in 0.1M phosphate buffer, pH 7.4. Brains were placed in a solution of 4% low melting agarose (Bio-Rad) and cut in coronal sections (80 μm) using a vibrating blade microtome (Leica VT1000S, Leica Microsystems). Sections were maintained in 0.01% azide-PBS buffer. For immunodetection, sections were blocked with 1X PBS with 2% normal donkey serum (Dominique Dutscher) and 0.3% Triton X-100 (PBS-T-NGS) for 30 minutes at room temperature. Primary antibodies were diluted in PBS-T-NGS and incubated overnight at 4°C. The following primary antibodies were used: anti-Dab1 (AB5840, rabbit, Millipore, 1:500), anti-p-Dab1 (sc-133292, rabbit, Santa Cruz, 1:50), anti-Cux1 (sc-13024, rabbit, Santa Cruz, 1:100), anti-Ki67 (IHC-00375, rabbit, Bethyl Laboratories, Inc, 1:250), anti-NEDD4L (13690-1-AP, rabbit, Proteintech, 1:300), anti-NeuN (MAB377, mouse, Millipore, 1:100), anti-Pax6 (PRB-278P, rabbit, Covance, 1:200),

anti-PH3 (06-570, rabbit, Millipore, 1:500) and anti-TBR2 (14-4875, rat, eBioscience, 1:200). After washes in 1X PBS, sections were incubated with Alexa Fluor conjugated secondary antibodies (A-31573 donkey anti-rabbit IgG 647, A-21208 donkey anti-rat IgG 488, A-21206 donkey anti-rabbit IgG 488, A-31571 donkey anti-mouse IgG 647; Life Technologies) diluted at 1:500 in PBS-T for 1h30 at room temperature. Sections were washed and then mounted with Fluoromount-G mounting medium (Interchim). All images were acquired using a TCS SP8 confocal microscope (Leica Microsystems) and positioning analysis was achieved with ImageJ software (NIH) and proliferation analysis with LAS AF software (Leica Microsystems). Graphs were made in GraphPad Prism 6 (GraphPad Software) and images were assembled with Adobe Photoshop 13.0.1 (Adobe Systems).

Ubiquitination assays

For immunoprecipitation assay, transfected cells were lysed with RIPA buffer supplemented with protease inhibitors (Roche), MG-132 (25 μM) and PR-619 (20mM) and protein extracts were incubated with anti-V5 agarose beads (A7345, Sigma) for 2 hours at 4°C under constant rotation in RIPA buffer. Immunoprecipitated proteins were eluted in Laemmli SDS buffer at 95°C and then subjected to SDS-PAGE. For in vitro ubiquitination assay, immunopurified NEDD4L from transfected N2A cells was incubated in reaction mixtures containing 200nM E1 ubiquitin-activating enzyme (BostonBiochem, Cambridge, MA), 400 nM E2 ubiquitin conjugating enzyme (UbcH7; BostonBiochem), 400 μM of ubiquitin (Sigma) and 2 mM ATP in a reaction buffer (25mM Tris/HCl (pH 7.5), 50 mM NaCl, 0.1 μM dithiothreitol and 4 mM $MgCl_2$). Reactions were incubated for 1hour at 30°C and analyzed by immunoblotting with anti-ubiquitin, anti-V5 and anti-NEDD4L antibodies.

In utero electroporation

In utero electroporation were performed as described previously13,40 using Swiss mice (Janvier). Animal experimentations were performed at the IGBMC animal facilities. The study has the Animal Experimentation Research Ethics Committee approval (N° 2014-059). Briefly, timed pregnant mice (E14.5) were anaesthetized with isoflurane (2 l per min of oxygen, 4% isoflurane during sleep and 2% isoflurane during surgery operation; Minerve). The uterine horns were exposed and a lateral ventricle of each embryo was injected using pulled glass capillaries with Fast Green (2 μg/ml; Sigma) combined with a final concentration of 1μg/μl of DNA constructs prepared by EndoFree plasmid purification kit (Macherey Nagel). The expression vector pCAGGS-Tomato was systematically co-electroporated and the fluorescent Tomato protein was used to visualize electroporated cells. Plasmids were further electroporated into the neuronal progenitors adjacent to the ventricle by delivering five electric pulses at 50V for 50ms at 950ms intervals using a CUY21EDIT electroporator (Sonidel Ltd). After electroporation, embryos were placed back in the abdominal cavity and development was allowed to continue until E16, E18 or P2. Embryos or pups brains were dissected and fixed in 4% PFA in PBS overnight.

Rapamycin treatment

Rapamycin Ready Made Solution (2.5 mg/ml in DMSO; Sigma) was previously diluted in PBS and then injected intraperitoneally at 0.5 mg/kg daily from E15.5 to E17.5 to pregnant females electroporated at E14.5 and embryos were collected at E18.5 for analysis.

Statistics

All statistics were calculated with GraphPad Prism 6 (GraphPad Software). Final counts are presented as the mean percentages ± standard error of the mean. One or two-way ANOVA were performed for multiple comparisons followed by Dunnett's or Sidak's post hoc tests respectively whereas unpaired two-tailed Student's *t*-test was used for dual comparisons. $P < 0.05$ was considered significant with $*P < 0.05$, $**P < 0.01$, $***P < 0.001$, $****P < 0.001$. Based on previous *in utero* electroporation experiments performed in our laboratory, we considered that at least 3 embryos per conditions would be necessary. After histological examination, only brains with comparative electroporated regions and efficiencies were conserved for quantification. One-way ANOVA test was used throughout the figures illustrating IUEP experiements to calculate all P values with $*P \leq 0.05$, $**P \leq 0.01$, $***P \leq 0.001$, $****P \leq 0.0001$. Data distribution was not tested but assumed to be normal. The investigator was not blinded for data collection and analysis. Statistical details were included in Supplementary Table 2.

Supplementary Material

Refer to Web version on PubMed Central for supplementary material.

Acknowledgments

We are grateful to the patients and their families for their participation. We Dr. Daniela Rotin and Dr Chong Jiang for kindely provinding humanV5-tagged Nedd4-2 constructs (pCDNA3.1-nV5 WT, CS and Y971A constructs), L Lindner and M Ruff (IGBMC, Strasbourg), M Macias (Institute for Research in Biomedicine, Barcelona) F. Francis (Institut du Fer à Moulin, Paris), for their thoughtful comments and help. We thank investigators from the Epi4K Consortium and the Epilepsy Phenome Genome Project for contributing NEDD4L-related genotype and phenotype data. This work was supported by funding from Strasbourg University and the Grant ANR-10-LABX-0030-INRT, a French State Fund managed by the Agence Nationale de la Recherche under the frame program Investissements d'Avenir ANR-10-IDEX-0002-02, the Fondation pour la Recherche Médicale (FRM funding within the frame of the programme Equipe FRM; J.C–DEQ20130326477), the Fondation Maladies Rares, Fondation NRJ – Institut de France, Agence National de Recherche (ANR Blanc 1103 01, project R11039KK; ANR E-Rare-012-01, project E10107KP; ANR-13-BSV-0009-01) and the EU-FP7 project GENECODYS (grant number 241995) and DESIRE (grant agreement 602531), and funding provided from the National Institute of Neurological Disorders and Stroke to the Epi4k Consortium and the Epilepsy Phenome/Genome Project (NS053998; NS077364; NS077274; NS077303 and NS077276). This study was also supported in part by the National Institute for Health Research (NIHR) Biomedical Research Centre Oxford with funding from the Department of Health's NIHR Biomedical Research Centre's funding scheme. The views expressed in this publication are those of the authors and not necessarily those of the Department of Health.

References

1. Caviness VS Jr, Takahashi T, Nowakowski RS. Numbers, time and neocortical neuronogenesis: a general developmental and evolutionary model. Trends Neurosci. 1995; 18:379–83. [PubMed: 7482802]
2. Rakic P, Caviness VS Jr. Cortical development: view from neurological mutants two decades later. Neuron. 1995; 14:1101–4. [PubMed: 7605626]
3. Barkovich AJ, Guerrini R, Kuzniecky RI, Jackson GD, Dobyns WB. A developmental and genetic classification for malformations of cortical development: update 2012. Brain: a journal of neurology. 2012; 135:1348–69. [PubMed: 22427329]
4. Francis F, et al. Human disorders of cortical development: from past to present. Eur J Neurosci. 2006; 23:877–93. [PubMed: 16519653]
5. Guerrini R, Dobyns WB. Malformations of cortical development: clinical features and genetic causes. Lancet Neurol. 2014; 13:710–26. [PubMed: 24932993]

6. Fox JW, et al. Mutations in filamin 1 prevent migration of cerebral cortical neurons in human periventricular heterotopia. Neuron. 1998; 21:1315–25. [PubMed: 9883725]
7. Parrini E, et al. Periventricular heterotopia: phenotypic heterogeneity and correlation with Filamin A mutations. Brain. 2006; 129:1892–906. [PubMed: 16684786]
8. Ferland RJ, et al. Disruption of neural progenitors along the ventricular and subventricular zones in periventricular heterotopia. Hum Mol Genet. 2009; 18:497–516. [PubMed: 18996916]
9. Carabalona A, et al. A glial origin for periventricular nodular heterotopia caused by impaired expression of Filamin-A. Hum Mol Genet. 2012; 21:1004–17. [PubMed: 22076441]
10. Lian G, et al. Filamin a regulates neural progenitor proliferation and cortical size through Wee1-dependent Cdk1 phosphorylation. J Neurosci. 2012; 32:7672–84. [PubMed: 22649246]
11. Sheen VL, et al. Mutations in ARFGEF2 implicate vesicle trafficking in neural progenitor proliferation and migration in the human cerebral cortex. Nat Genet. 2004; 36:69–76. [PubMed: 14647276]
12. Conti V, et al. Periventricular heterotopia in 6q terminal deletion syndrome: role of the C6orf70 gene. Brain. 2013; 136:3378–94. [PubMed: 24056535]
13. Poirier K, et al. Mutations in TUBG1, DYNC1H1, KIF5C and KIF2A cause malformations of cortical development and microcephaly. Nat Genet. 2013; 45:639–47. [PubMed: 23603762]
14. Mirzaa GM, et al. Characterisation of mutations of the phosphoinositide-3-kinase regulatory subunit, PIK3R2, in perisylvian polymicrogyria: a next-generation sequencing study. Lancet Neurol. 2015; 14:1182–95. [PubMed: 26520804]
15. Kumar S, Tomooka Y, Noda M. Identification of a set of genes with developmentally down-regulated expression in the mouse brain. Biochem Biophys Res Commun. 1992; 185:1155–61. [PubMed: 1378265]
16. Sudol M, Chen HI, Bougeret C, Einbond A, Bork P. Characterization of a novel protein-binding module--the WW domain. FEBS Lett. 1995; 369:67–71. [PubMed: 7641887]
17. Rizo J, Sudhof TC. C2-domains, structure and function of a universal Ca2+-binding domain. J Biol Chem. 1998; 273:15879–82. [PubMed: 9632630]
18. Huang L, et al. Structure of an E6AP-UbcH7 complex: insights into ubiquitination by the E2-E3 enzyme cascade. Science. 1999; 286:1321–6. [PubMed: 10558980]
19. Goel P, Manning JA, Kumar S. NEDD4-2 (NEDD4L): the ubiquitin ligase for multiple membrane proteins. Gene. 2014; 557:1–10. [PubMed: 25433090]
20. Garrone NF, Blazer-Yost BL, Weiss RB, Lalouel JM, Rohrwasser A. A human polymorphism affects NEDD4L subcellular targeting by leading to two isoforms that contain or lack a C2 domain. BMC Cell Biol. 2009; 10:26. [PubMed: 19364400]
21. Hsia HE, et al. Ubiquitin E3 ligase Nedd4-1 acts as a downstream target of PI3K/PTEN-mTORC1 signaling to promote neurite growth. Proc Natl Acad Sci U S A. 2014; 111:13205–10. [PubMed: 25157163]
22. Franco SJ, Martinez-Garay I, Gil-Sanz C, Harkins-Perry SR, Muller U. Reelin regulates cadherin function via Dab1/Rap1 to control neuronal migration and lamination in the neocortex. Neuron. 2011; 69:482–9. [PubMed: 21315259]
23. Olson EC, Kim S, Walsh CA. Impaired neuronal positioning and dendritogenesis in the neocortex after cell-autonomous Dab1 suppression. J Neurosci. 2006; 26:1767–75. [PubMed: 16467525]
24. Sekine K, Honda T, Kawauchi T, Kubo K, Nakajima K. The outermost region of the developing cortical plate is crucial for both the switch of the radial migration mode and the Dab1-dependent “inside-out” lamination in the neocortex. J Neurosci. 2011; 31:9426–39. [PubMed: 21697392]
25. Sekine K, et al. Reelin controls neuronal positioning by promoting cell-matrix adhesion via inside-out activation of integrin alpha5beta1. Neuron. 2012; 76:353–69. [PubMed: 23083738]
26. Lifton RP, Gharavi AG, Geller DS. Molecular mechanisms of human hypertension. Cell. 2001; 104:545–56. [PubMed: 11239411]
27. Boase NA, Kumar S. NEDD4: The founding member of a family of ubiquitin-protein ligases. Gene. 2015; 557:113–22. [PubMed: 25527121]
28. Moon UY, et al. Impaired Reelin-Dab1 Signaling Contributes to Neuronal Migration Deficits of Tuberous Sclerosis Complex. Cell Rep. 2015; 12:965–78. [PubMed: 26235615]

29. Gao S, et al. Ubiquitin ligase Nedd4L targets activated Smad2/3 to limit TGF-beta signaling. Mol Cell. 2009; 36:457–68. [PubMed: 19917253]
30. Yu JS, et al. PI3K/mTORC2 regulates TGF-beta/Activin signalling by modulating Smad2/3 activity via linker phosphorylation. Nat Commun. 2015; 6:7212. [PubMed: 25998442]
31. Wiesner S, et al. Autoinhibition of the HECT-type ubiquitin ligase Smurf2 through its C2 domain. Cell. 2007; 130:651–62. [PubMed: 17719543]
32. Bruce MC, et al. Regulation of Nedd4-2 self-ubiquitination and stability by a PY motif located within its HECT-domain. Biochem J. 2008; 415:155–63. [PubMed: 18498246]
33. Wang J, et al. Calcium activates Nedd4 E3 ubiquitin ligases by releasing the C2 domain-mediated auto-inhibition. J Biol Chem. 2010; 285:12279–88. [PubMed: 20172859]
34. Escobedo A, et al. Structural basis of the activation and degradation mechanisms of the E3 ubiquitin ligase Nedd4L. Structure. 2014; 22:1446–57. [PubMed: 25295397]
35. Honda T, Nakajima K. Proper Level of Cytosolic Disabled-1, Which Is Regulated by Dual Nuclear Translocation Pathways, Is Important for Cortical Neuronal Migration. Cereb Cortex. 2015
36. Riviere JB, et al. De novo germline and postzygotic mutations in AKT3, PIK3R2 and PIK3CA cause a spectrum of related megalencephaly syndromes. Nat Genet. 2012; 44:934–40. [PubMed: 22729224]
37. Jansen LA, et al. PI3K/AKT pathway mutations cause a spectrum of brain malformations from megalencephaly to focal cortical dysplasia. Brain. 2015; 138:1613–28. [PubMed: 25722288]
38. Wright CF, et al. Genetic diagnosis of developmental disorders in the DDD study: a scalable analysis of genome-wide research data. Lancet. 2015; 385:1305–14. [PubMed: 25529582]
39. Cau E, Gradwohl G, Fode C, Guillemot F. Mash1 activates a cascade of bHLH regulators in olfactory neuron progenitors. Development. 1997; 124:1611–21. [PubMed: 9108377]
40. Kielar M, et al. Mutations in Eml1 lead to ectopic progenitors and neuronal heterotopia in mouse and human. Nat Neurosci. 2014; 17:923–33. [PubMed: 24859200]

Europe PMC Funders Author Manuscripts

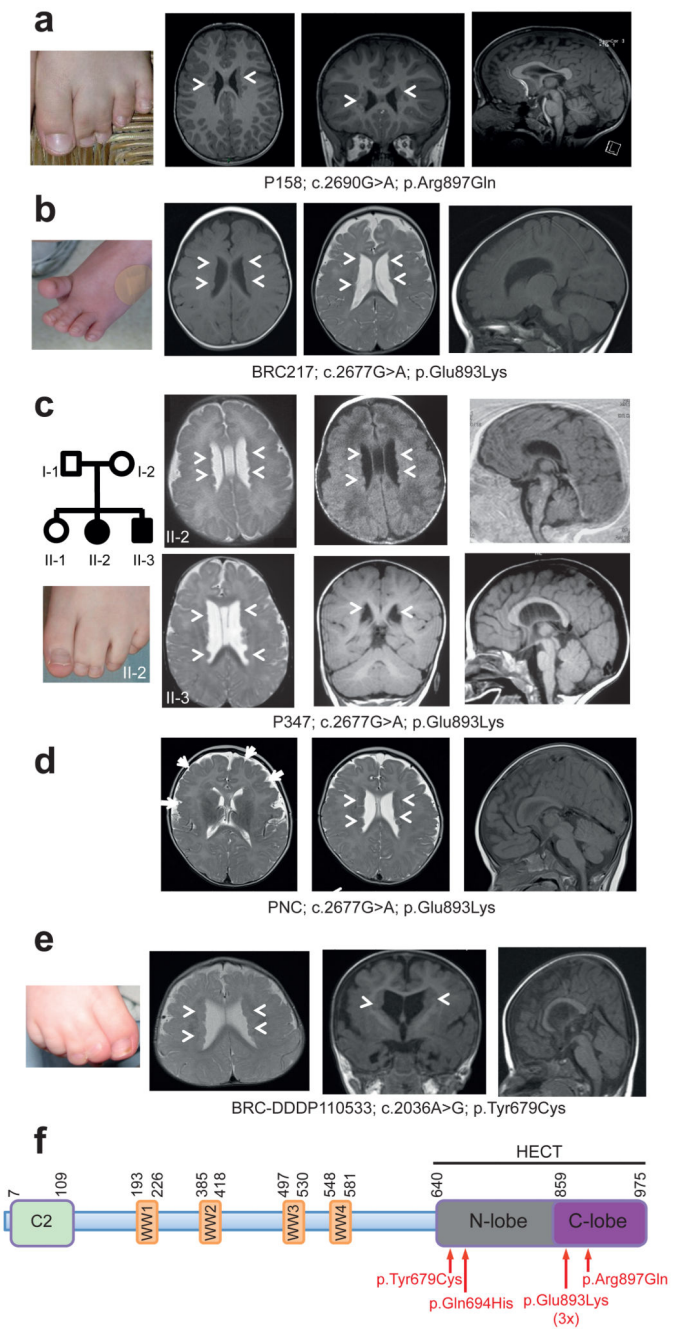

Figure 1.

Mutations in *NEDD4L* cause PNH and syndactyly. (**a-e**) Photographs and representative sections of brain magnetic resonance imaging (MRI) of affected individuals illustrating the frequent toes syndactyly and the constant PNH. For each patient, two axial sections, or one axial and one coronal section show confluent nodules of heterotopia lining the lateral ventricles, (arrowsheads). Sagittal sections show thin (c) or dysmorphic (c, II-3 and a) corpus callosum. In (d), in addition to the PNH (arrowheads), MRI section shows frontal polymicrogyria (white arrows). MRIs were performed at the age of 8 years (a), 12 months

(b), 9 and 12 months (c), 7 months (d) and 8 months (e). For the patient Pnh31124 with the c.2082G>T; p.Gln694His mutation, MR images were not available. (**f**) Linear representation of NEDD4L polypeptide showing positions in the HECT domain of the heterozygous PNH-associated mutation. NEDD4L protein is characterized by an N-terminal C2 domain known to bind Ca^{2+} and phospholipids17, 2 to 4 WW protein-protein interacting domains16 responsible for the recognition of the substrate, and the C-terminal catalytic HECT domain18.

Europe PMC Funders Author Manuscripts

Europe PMC Funders Author Manuscripts

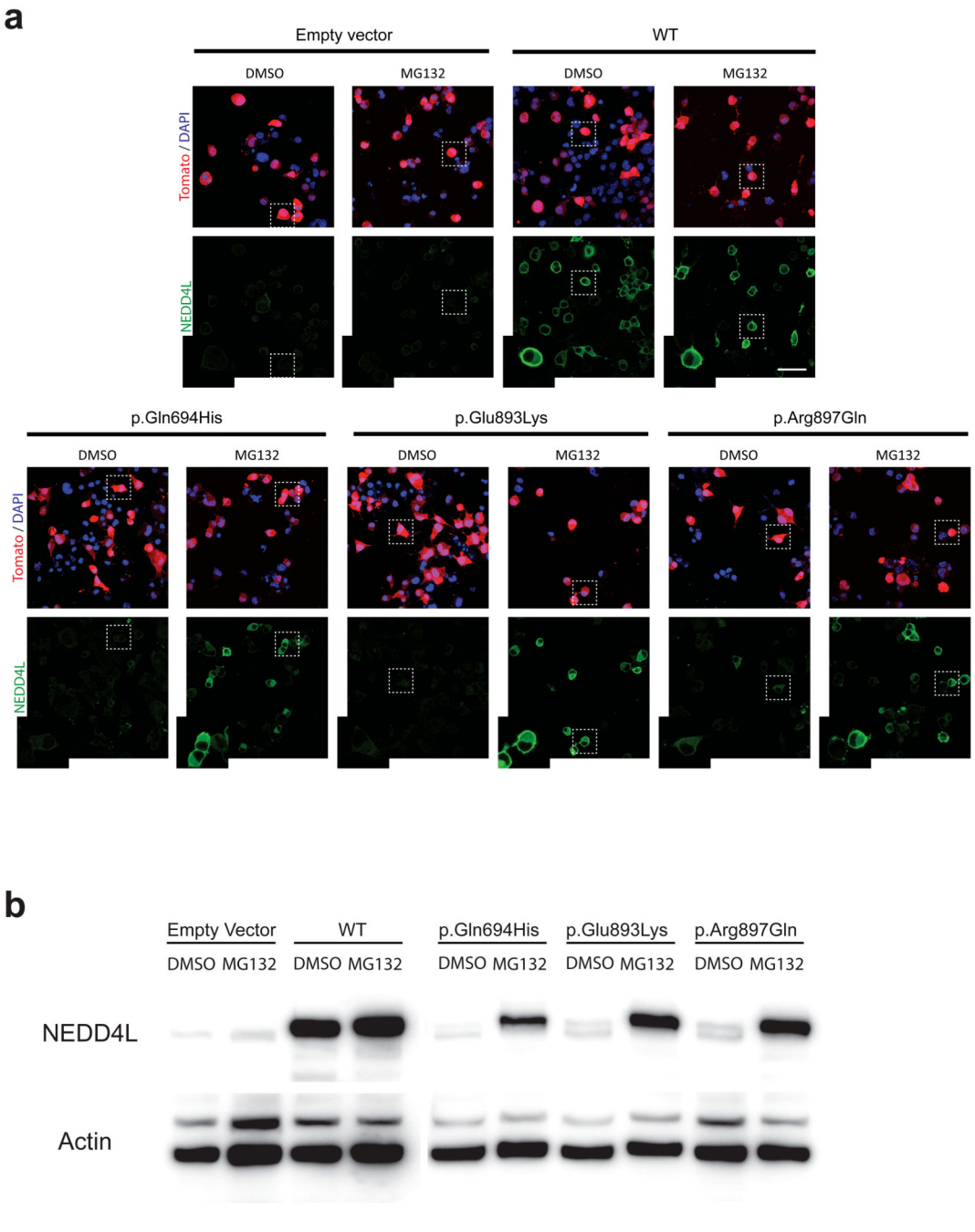

Figure 2.

Expression and cellular localization of WT and NEDD4L mutants. (**a**) Tomato/DAPI and NEDD4L detection in N2A cells transfected with empty vector, WT and mutant *NEDD4L* cDNA constructs. For each construct, cultured cells were either treated with DMSO or with MG132. NEDD4L immunostaining (green) shows a cytoplasmic distribution, with enrichment in the periphery of N2A cells, of WT NEDD4L, whereas p.Gln694His, p.Glu893Lys and p.Arg897Gln mutants are not detectable. (**b**) Western blots using protein extracts of N2A cells transfected with WT and *NEDD4L* mutants and cultured either in

presence of DMSO or MG132. They show the lack of expression of PNH-associated mutants, while transfection of WT lead to a significant expression of NEDD4L protein. Note that PNH-associated NEDD4L mutants become detectable upon treatment of N2A cells with MG132.

Europe PMC Funders Author Manuscripts

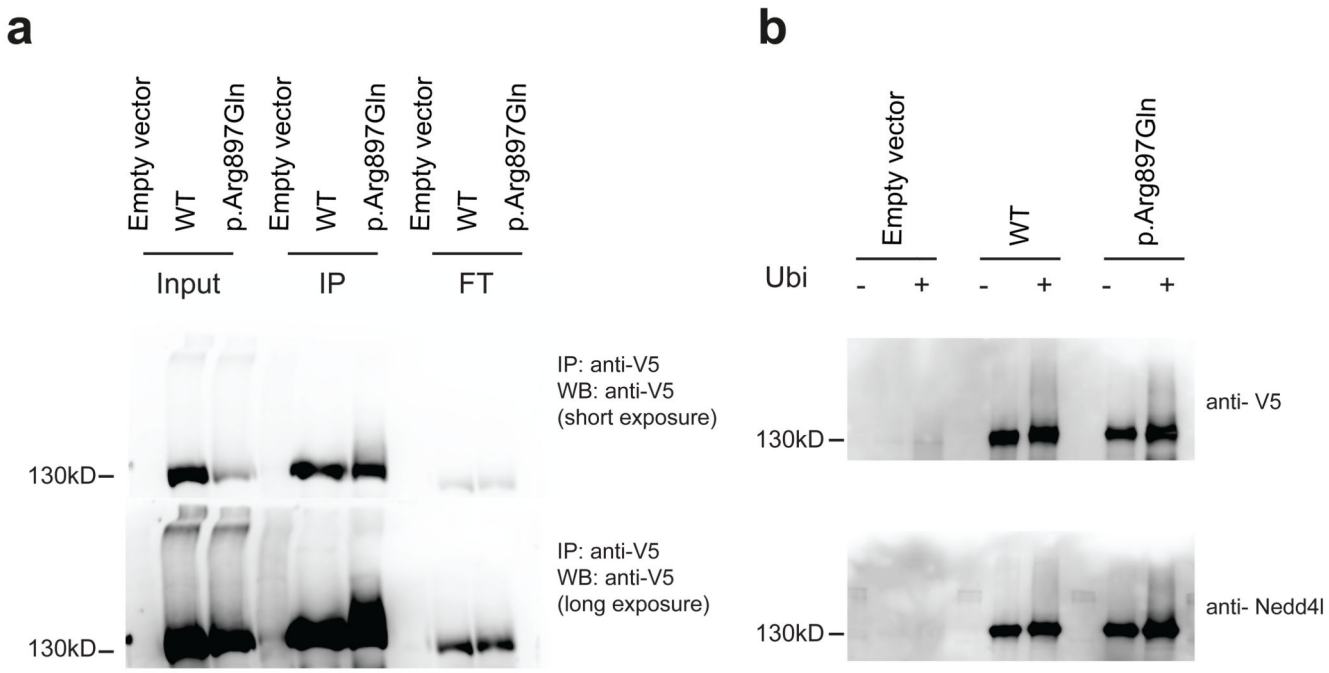

Figure 3.

Ubiquitination activity of NEDD4L mutant. (**a**) Immunoprecipitation assay (using anti-V5 antibody to precipitate tagged NEDD4L) analyzed by immunoblots using anti-ubiquitin, anti-V5 antibodies to detect ubiquitinated NEDD4L. (**b**) Analysis of NEDD4L ubiquitination activity in an *in vitro* assay using WT and NEDD4L mutant immunopurified from transfected N2A cell lysates and incubated with ATP, E1 enzyme and E2 (UbcH7) enzyme with (+) or without (-) ubiquitin. Reaction mixtures were analyzed by immunoblotting using anti-V5 and anti-NEDD4L antibodies. Note that because of the instability of mutant NEDD4L and the resulting unbalanced amounts of WT and NEDD4L mutant and immunoblot signals as shown in Supplementary Figure 7, Western blot analysis was performed using four times less of reaction mixture corresponding to WT NEDD4L than to NEDD4L mutant.

Europe PMC Funders Author Manuscripts

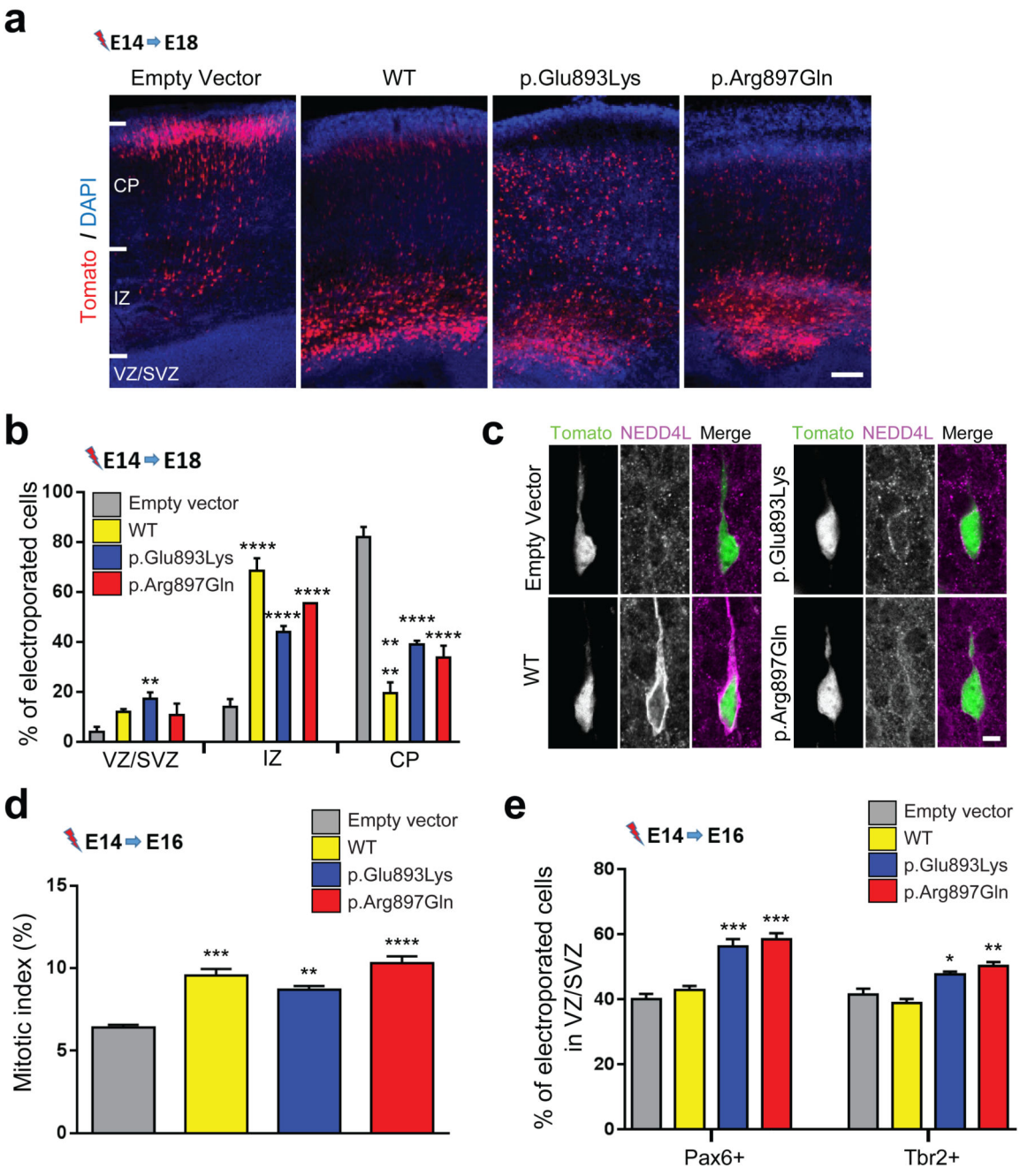

Figure 4.

Effect of WT and NEDD4L mutants on neuronal position and progenitors proliferation. (**a**) Coronal sections of mouse brains at E18.5, 4 days after IUEP with empty vector (EV), WT *NEDD4L*, or *NEDD4L* mutant constructs in combination with a Tomato reporter construct. CP, cortical plate; IZ intermediate zone; VZ/SVZ ventricular zone/subventricular zone. Scale bar, 100 μm. (**b**) Fluorescent neurons were quantified in the regions highlighted in (a): VZ/SVZ: EV vs p.Glu893Lys, P = 0.0078; IZ: EV vs WT, P < 0.0001, EV vs p.Glu893Lys, P<0.0001, EV vs p.Arg897Gln, P < 0.0001; CP: EV vs WT, P < 0.0001, EV vs

p.Glu893Lys, P < 0.0001, EV vs p.Arg897Gln, P<0.0001. Bars represent the mean of fluorescent neurons ± s.e.m. of independent brains (EV, n = 4; WT, n=3; p.Glu893Lys, n = 4; p.Arg897Gln, n = 3). (**c**) Immunofluorescence staining of NEDD4L (magenta) in tomato positive neurons (green) in IZ of E18.5 brains electroporated at E14.5 with *NEDD4L* constructs. Scale bar 5 μm. (**d**) Percentage of electroporated neurons positive for PH3 marker against all electroporated cells (mitotic index) in the VZ (Fig. 4a and Supplementary Fig. 9d): EV vs WT, P < 0.0001, EV vs p.Glu893Lys, P = 0.0021, EV vs p.Arg897Gln, P = 0.0001. Number of analyzed brains are as follows: EV, n = 4; WT, n = 3; p.Glu893Lys, n = 4; p.Arg897Gln, n = 3). (**e**) Quantification of Pax6+/Tomato+ and Tbr2+/Tomato+ cells in the VZ/SVZ (Fig. 4a and Supplementary Fig. 9e) two days after electroporation at E14.5: Pax6: EV vs p.Glu893Lys, P = 0.0003, EV vs p.Arg897Gln, P = 0.0001; Tbr2: EV vs p.Glu893Lys, P = 0.0147, EV vs p.Arg897Gln, P = 0.0014. (EV, n = 4; WT, n = 3; p.Glu893Lys, n = 4; p.Arg897Gln, n = 3). Error bars represent s.e.m.

Europe PMC Funders Author Manuscripts

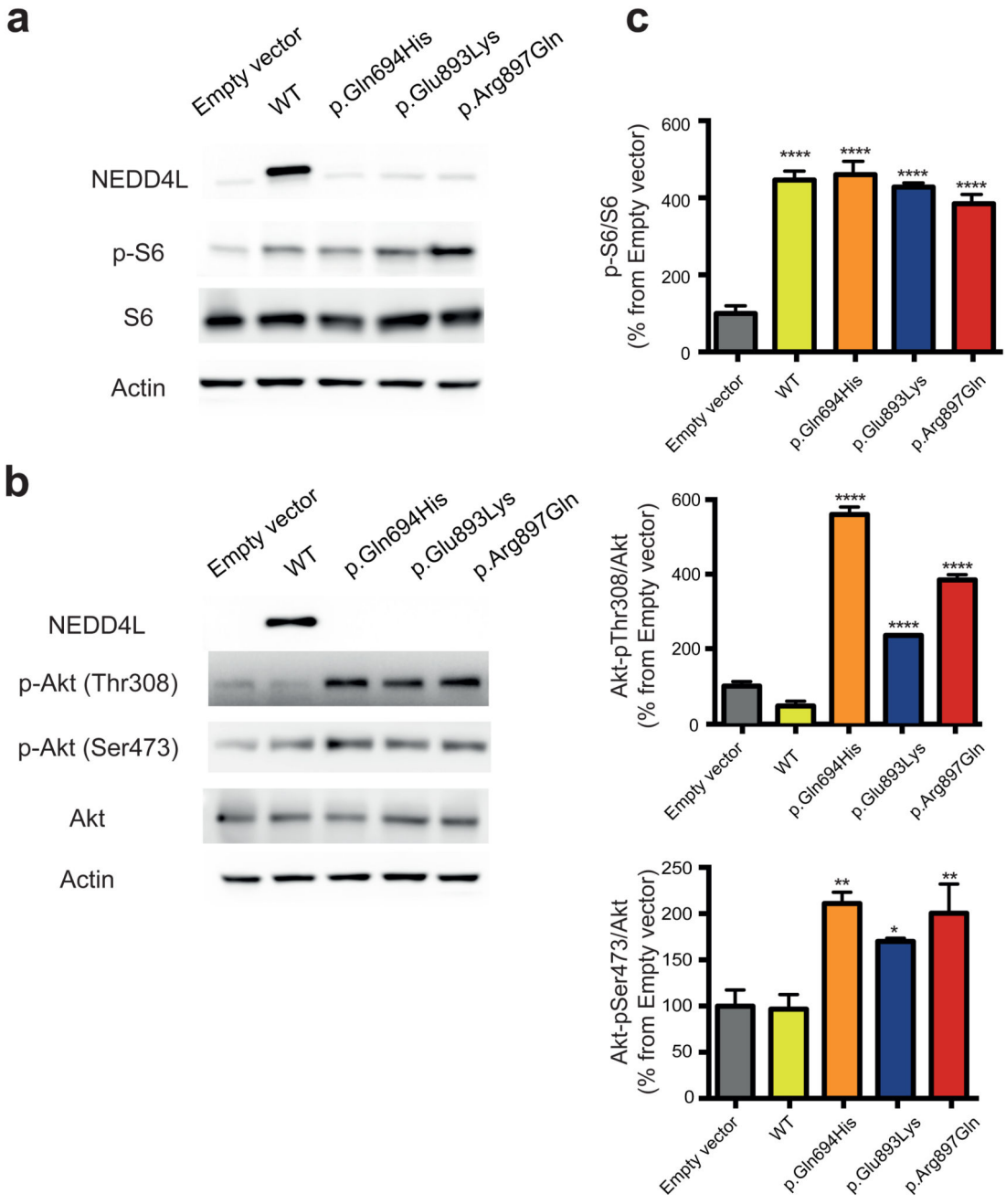

Figure 5.

WT NEDD4L and PNH-related mutants induce deregulation of mTORC1 and AKT activities. (**a,b**) Representative immunoblots using protein extracts of N2A cells transfected with empty vector, WT and *NEDD4L* mutant constructs, and showing the effect of the WT and NEDD4L mutants on p-S6 level (phosphorylated S6 that reflects mTORC1 activity) and p-Akt (Thr308/Ser473). (**c**) Histograms of densitometric measurements illustrating S6 and Akt phosphorylation. Data represent mean ± sem of three independent experiments. *p≤0.05, **p≤0.01, ***p≤0.001, ****p≤0.0001

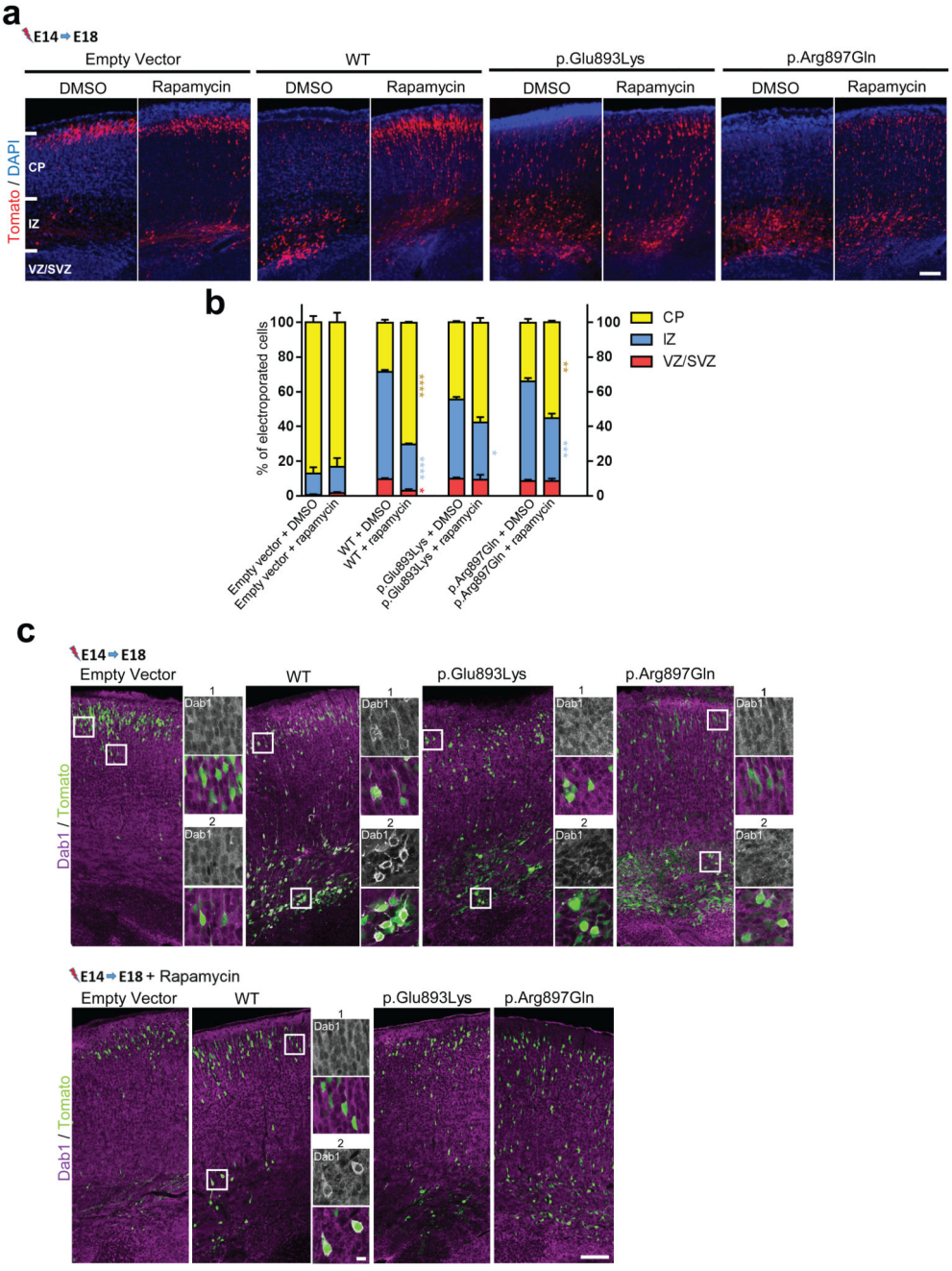

Figure 6.

Effect of rapamycin treatment on neuronal positioning and Dab1 localization. (**a**) Confocal microscope images of coronal sections from E18.5 brains electroporated at E14.5 with either empty vector, WT *NEDD4L*, or mutants *NEDD4L*, and the Tomato reporter vector. Following IUEP, pregnant mice were either treated with vehicle (DMSO) or with rapamycin (0.5 mg/kg/day). CP, cortical plate; IZ intermediate zone; VZ/SVZ ventricular zone/ subventricular zone. Scale bar 100 μm. (**b**) Electroporated neurons were quantified in the regions indicate in (a): VZ/SVZ: WT DMSO vs WT Rapamycin, P=0.012, IZ: WT DMSO

Europe PMC Funders Author Manuscripts

vs WT Rapamycin, P<0.0001; CP: WT DMSO vs WT Rapamycin, P<0.0001); IZ: p.Glu893Lys DMSO vs p.Glu893Lys Rapamycin, P=0.0377, p.Arg897Gln DMSO vs p.Arg897Gln Rapamycin, P=0.0004; CP : p.Arg897Gln DMSO vs p.Arg897Gln Rapamycin, P=0.0013. Bars represent the mean of electroporated neurons in each regions ± s.e.m. of 3 independent brains. (**c**) Immunolabelings of Dab1 (magenta) on cortical slices at E18.5 from brain embryos subjected to DMSO or rapamycin treatment. Right panels of each coronal section are higher magnifications of white boxes in the CP (1) and IZ (2) showing the distribution of Dab1. In arrested neurons electroporated with WT *NEDD4L* of non-treated mice, note the specific pattern of Dab1 distribution and its enrichment in the periphery of the cytoplasm (mainly in arrested neurons of the IZ and to a less extend in neurons of the cortical plate). Scale bar 100 μm; 10 μm (higher magnifications).

Europe PMC Funders Author Manuscripts

Europe PMC Funders Author Manuscripts

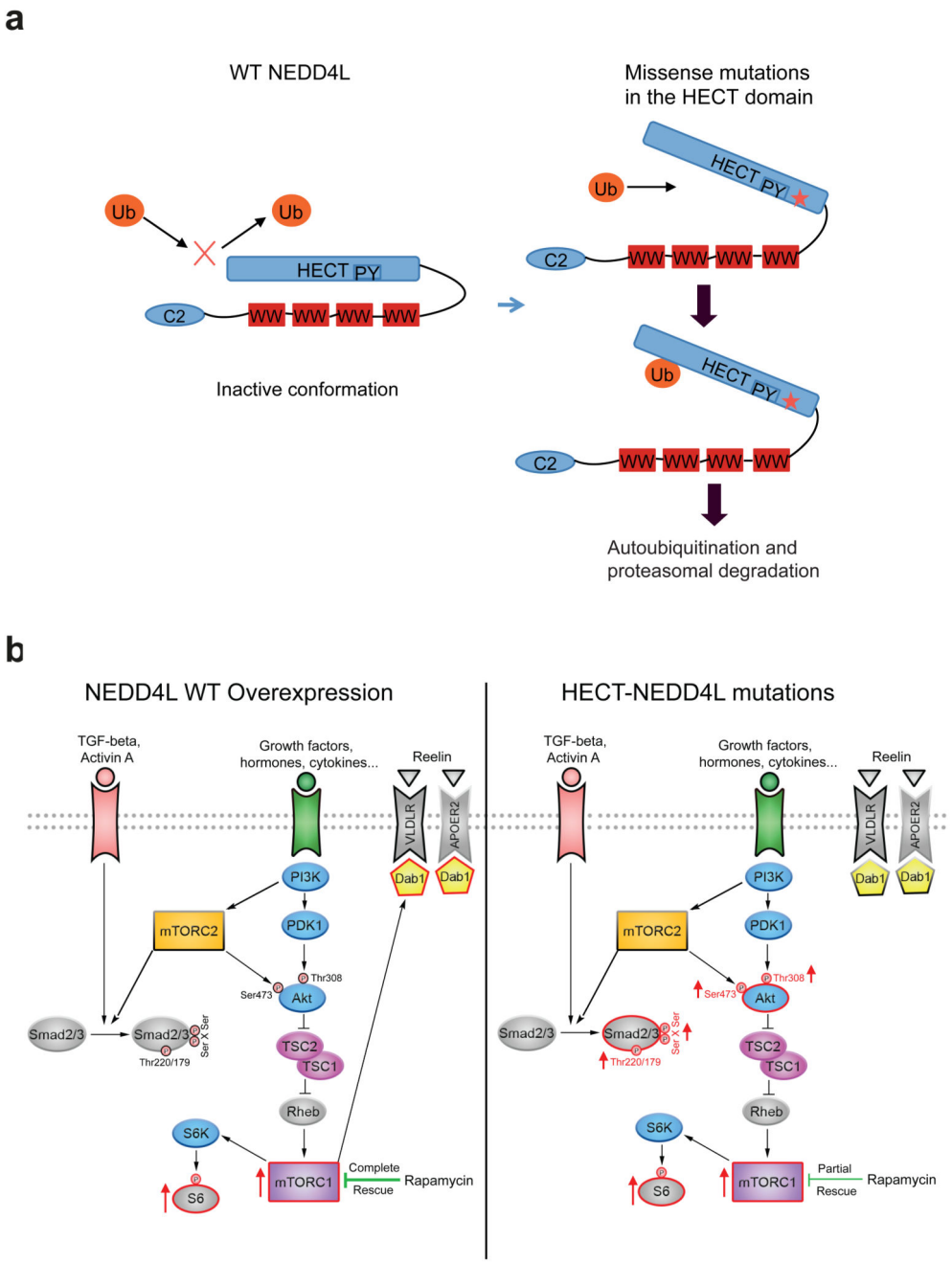

Figure 7.

Models depicting consequences of PNH-related mutations on NEDD4L stability and PI3K/Akt/mTOR and TGF-β/Smad pathways. (**a**) WT NEDD4L (on the left) is shown in its closed and inactive conformation, and NEDD4L mutant (on the right) with an alteration in the HECT domain predicted to lead to conformation changes that favours transition from inactive to open active state and triggers auto-ubiquitination and degradation. (**b**) Overview of observed deregulations in basal conditions resulting from an excess of WT NEDD4L (on the left) and expression PNH-related NEDD4L mutants (on the right). Red contours indicate

deregulated proteins and dotted arrows depict indirect and poorly understood relations between partners of signaling pathways.

Europe PMC Funders Author Manuscripts

Europe PMC Funders Author Manuscripts

Table 1

Summary of clinical and neuroimaging features of patients harbouring NEDD4L mutations.

Patients with PNH	**P158 c.2690G>A p. Arg897Gln**		**P347 c.2677G>A p.Glu893Lys**	**BRC217 c.2677G>A p.Glu893Lys**	**PNC c.2677G>A p.Glu893Lys**	**Pnh31124 c.2082G>T p.Gln694His**	**DDDP110533 c.2036A>G Tyr679Cys**
		P347-II.2	**P347-II.3**				
Inheritance	*De novo*	Maternal mosaicism	Maternal mosaicism	*De novo*	*De novo*	*De novo*	*De novo*
Sex	M	F	M	F	F	F	M
Birth – GW	40	41	41	41	38	Full term	40
Birth weight	3750	3160	NA	3120	3360	NA	3000
Syndactyly	+	+	+	+	-	+	+
hypotonia	+ at birth	NA	NA	+ + (at 2 months)	+ axial hypotonia at 34 months	+	+ unable to sit or walk at 6 years
Cleft palate	-	+	bifid uvula	+	+	+	+ and micrognathia
age at last examination	6 years	12 years	2 years	4 months	4 years	8 months	6.2 years
HC (cm)	54 (+1.5 SD)	50 (-2.4 SD)	49.8 (+0.7 SD)	39 (-1.2 SD)	48 (-1.2 SD)	43 (-1 SD)	49.7(-2.32 SD)
Height (cm)	1.08 (- 1.5 SD)	125 (-3.5 SD)	88 (+0.8 SD)	61 (M)	100 (+2 SD)	68 (-0.5 SD)	NA
Weight (kg)	16.5 (-1.5 SD)	25 (-2.5 SD)	10.9 (+0.7 SD)	5.29 (-1.1 SD)	14 (-0.8 SD)	7.6 (-2 SD)	20 (-0.51SD)
Developmental delay	+	+ (severe)	+ (severe)	+	+	+	+ (severe)
Seizures	-	+ (late onset)	+	-	-	+ IS at 5 months	+
Brain MRI Findings	At 8 years	At 9 months	At 2 months	At 12 months	At 7 months	At 8 months	At 8 months
PNH	+ (bilateral)	+ (bilateral)	+ (bilateral)	+ (bilateral)	+ (bilateral)	+ (bilateral)	+ (bilateral)
CC anomalies	-	-	-	Dysmorphic	Dysmorphic	-	-
Cortex anomalies	-	Cerebral atrophy	-	Frontal cortical dysplasia	PMG	-	-
Cerebellum anomalies	-	-	-	-	-	-	-
Other	Myopia	Optic atrophy Hearing impairment	Convergent Strabismus cryptorchidism	Hearing impairment,	dysmorphic features	Abnormal visual evoked potentials, optic nerve pallor	Arthrogyposis, cryptorchidism, ptosis, complex strabismus

PNH, periventricular nodular heterotopia; PMG, polymycrogyria; CC, Corpus callosum; GW, gestational week; HC, head circumference; IS, infantile spasm; NA, not available; +, present; −, absent. Transcript NM_001144967.2 (ENST00000400345) and protein Q96PU5 were used for the nomenclature of nucleotide and protein changes.